PROCESS INTERMITTENT MEASUREMENT FOR POWDER-BED BASED ADDITIVE MANUFACTURING

A.L. Cooke[*†], S.P. Moylan[*]

[*]National Institute of Standards and Technology, Gaithersburg, MD 20899[1]
[†]Institute for Research in Electronics and Applied Physics, University of Maryland, College Park, MD 20742-3511

Abstract

Process intermittent measurements of parts fabricated by additive manufacturing (AM) can enable both process improvement and characterization of internal part geometries. The planar, layer-upon-layer nature of most AM processes allows two-dimensional geometric measurements with a vision system, because the part's current layer is continually in focus. Proof of this concept has been shown through measurement of parts made using a three-dimensional (3D) printer. Process intermittent measurements were compared to contact and non-contact measurements of the finished parts to characterize deviations in printed layer positions and changes in part dimensions resulting from post-process treatments.

Introduction

Powder-bed based AM methods include powder bed fusion processes, during which thermal energy selectively fuses regions of a powder bed, and binder-jetting processes, during which a liquid bonding agent is selectively deposited to join powder materials in a bed. 3D printing is a binder-jetting process that is the topic of this paper. It is a method in which primarily starch-based materials can be joined with clear or colored binder to produce 3D parts. As with all powder bed based processes, layers of powder are spread to cover a build platform to allow single cross sections (or layers) of the part to be produced. This planar, layerwise nature of the process allows two dimensional (2D) optical measurements of the bonded layer geometry to be made intermittently for all layers. Calibration, which includes determination of measurement uncertainty of the optical system, enables quantitative comparisons to be made between geometries and measurements. This method of *in-situ* part inspection is a form of real-time non-destructive analysis (NDA), which was identified as a research opportunity by the 2009 *Roadmap for Additive Manufacturing* [1]. Previous research has incorporated an optical system to perform real-time NDA of the 3D printing process in order to map the internal structures of the 3D part being built [2]. This current study is a first step in developing a closed-loop control system for a metal-based AM machine, which will monitor the part being made and communicate necessary information to the machine's controller to alter process parameters to

---

ensure part quality. Process intermittent metrology is likely to be more valuable for metallic parts than non-metal parts because of the higher inherent value and accuracy requirements of those parts. In order to verify that in-process measurements can meaningfully predict the characteristics of the final part, comparisons were made between the process intermittent images and measurements of the finished parts before and after post-process treatment, *i.e.*, adding infiltrant. This will help define the relationship between intermittent measurements of parts and the final part geometry after it has undergone any changes in dimensions due to the post-process treatments.

Test Parts

Several iterations of the test part were developed and constructed before the final design was determined. The part was designed not to assess the performance of the machine, but rather to allow characterization of the measurement process. Images of the actual part and the top, front, and left side views of the solid model are shown in Figure 1.
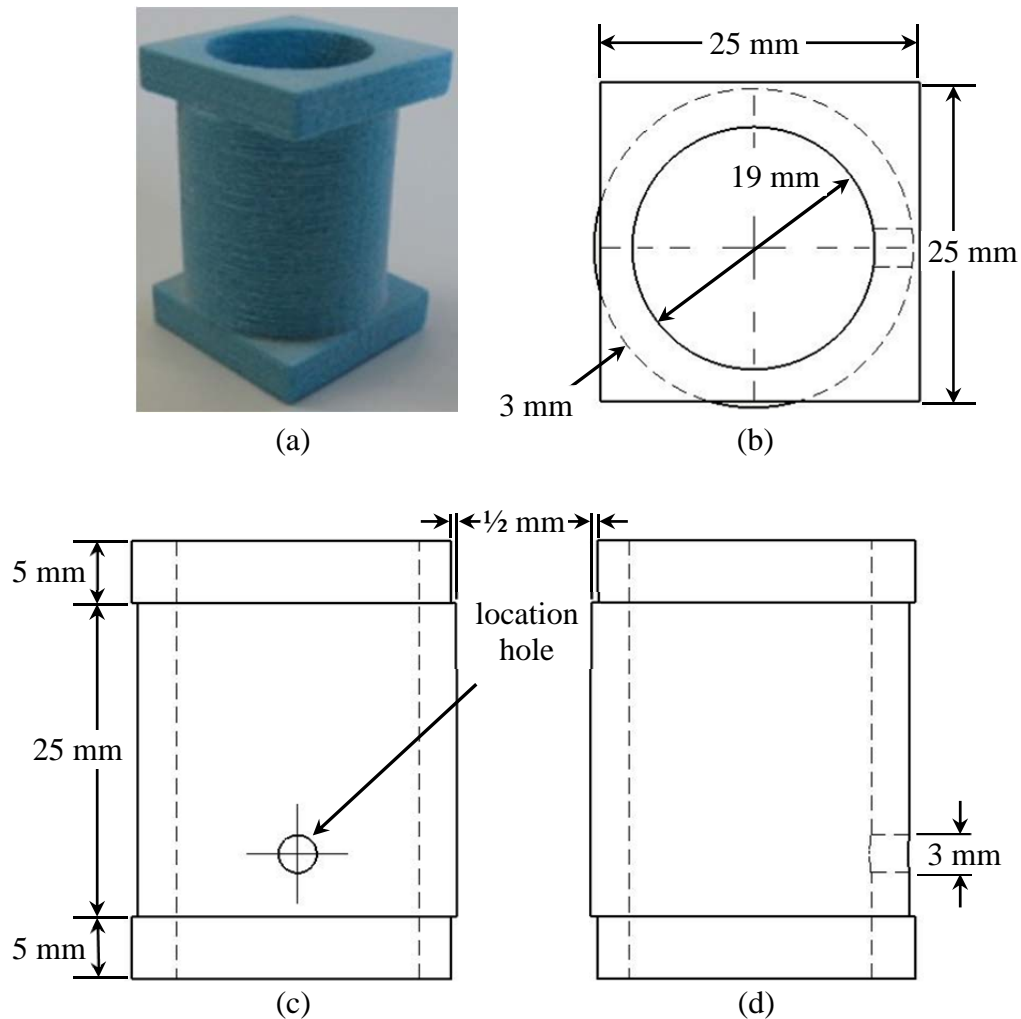
Figure 1: Image of the (a) actual part and (b) top, (c) front, and (d) left side views of the solid model.

The test part is 25 mm wide, 25 mm deep, 35 mm tall, and is comprised of three sections: the top and bottom platens, both of which are 5 mm thick, and the middle cylinder, which is 25 mm tall. The cylinder has a 3 mm wall thickness and a location hole placed at the front of the part to enable consistent orientation when preparing print jobs on the 3D printer and measuring parts post-process. Additionally, the central axis of the cylinder is offset by half of a millimeter to create an overhang on the right side and back of the artifact. This offset provides a reference step in profilometer measurement data during post-process analysis. The bottom platen is built into the design to provide corners with which to affix the part to the table surface of a coordinate measuring machine (CMM) with clay. The top platen was added so that the artifact could lie flatly on its front or left side, facilitating horizontal post-process measurement methods. The part is cyan in color so that during printing only one printhead was utilized. This way, any printhead error encountered while printing could be traced back to this one printhead. The color also showed up well in the camera images, as discussed later. The individual layer thickness used during the print jobs was nominally 0.100 mm.

Equipment

Printer

The 3D printer used in this research has a build size of 254 mm x 356 mm x 203 mm, capable layer thicknesses ranging from 0.089 mm to 0.203 mm, and a resolution of 23.6 dots per mm x 21.6 dots per mm (600 dots per inch x 540 dots per inch). The powder and binder supplied with the machine (ZP131 and ZB60, respectively) were used to print the test parts. The software used to program the 3D printer virtually slices the 3D computer-aided design (CAD) file into numerous 2D slices and sends them to the 3D printer to be printed. The software supports various types of files, including virtual reality modeling language (vrml) files, which were used in this research. This file format includes color information and is supported by the 3D modeling software used to design the test part. The 3D printer software allows the user to utilize a tool called bleed compensation. This feature takes into account the amount that the binder will spread through the material, which could result in slightly oversized parts, and "shaves" off a small amount of each dimension to compensate. The compensation values used were the default values. Additionally, the software also indicates when to print shell and core portions of the part. The shell and core saturations can be varied, and in this research, values of 100 percent were maintained for both. The various parameters and options used for the printing of the test parts are listed in Table 1.

Table 1: Options and parameters used for test parts.

Description	Option/Value
Powder	ZP131
Binder	ZB60
Layer Thickness (mm)	0.100
Shell Saturation (%)	100
Core Saturation (%)	100
Bleed Compensation, X (mm)	0.11430
Bleed Compensation, Y (mm)	0.09652
Bleed Compensation, Z (mm)	0.06858

Imaging System

The camera used for this research was a charge-coupled device (CCD) digital camera with a 1.23 Mega-pixel array, a high-speed IEEE1394 interface, and an external triggering capability. The pixel array provides a frame size of 1280 pixels x 960 pixels. The lens attached to the camera was a close focus zoom lens with a C-mount. The manual zoom lens provided a variable working distance of 152 mm to 457 mm, a variable focal length of 13 mm to 130 mm, and a variable field of view of 7.8 mm to 280 mm. The 16-bit images acquired by this device are grayscale. A calibration plate was imaged at each magnification setting used in this study. Images acquired for the three magnifications used here are displayed in Figure 2. The three magnifications correspond to 0.049 mm/pixel for magnification A, 0.023 mm/pixel for magnification B, and 0.010 mm/pixel for magnification C. The displayed images represent layer 200 of each build cycle.


(a)

(b)

(c)
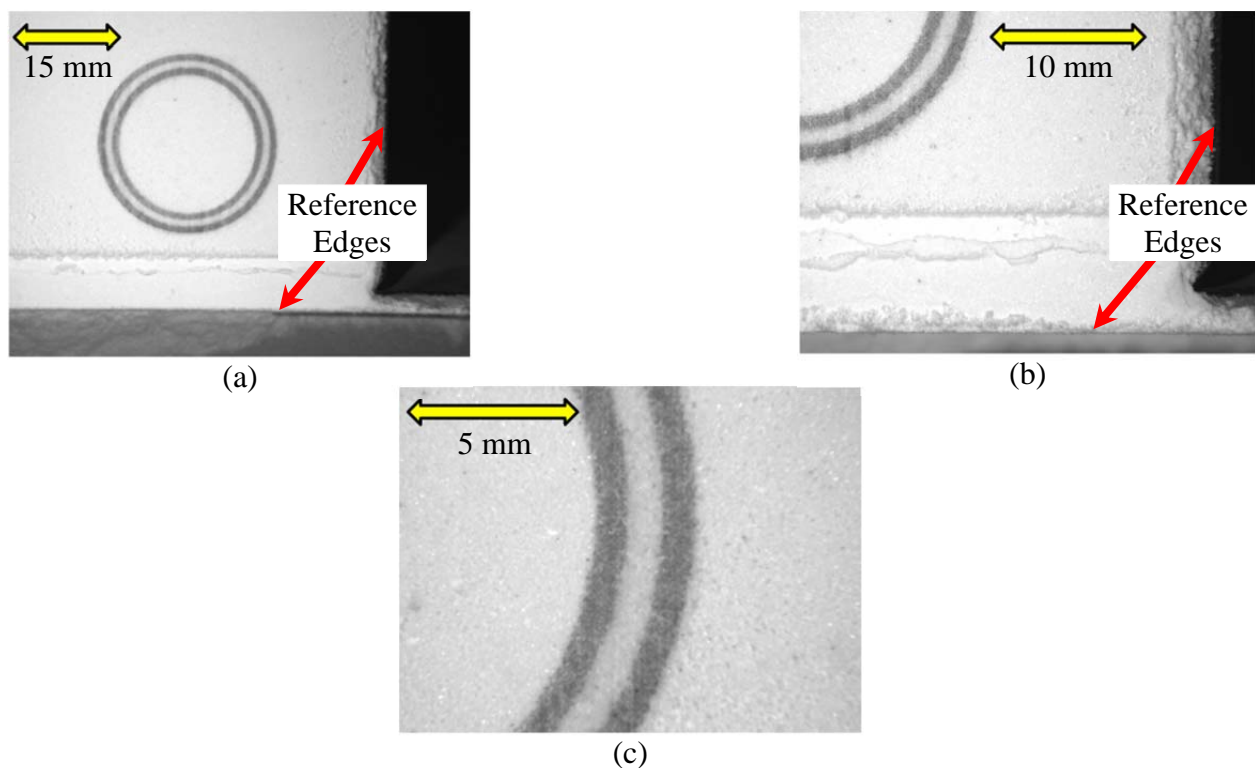
Figure 2: Images taken at magnifications (a) A, (b) B, and (c) C.

Magnification A was chosen because the image contains the entire part as well as reference edges (*i.e.*, the edges of the build bed). Magnification B was chosen to improve the resolution of the images while still capturing reference edges within the field of view. Magnification C was chosen to maximize the resolution without having to reposition the camera system.

The vision system was positioned on the top of the printer by means of a custom-made mounting fixture. The apparatus required the removal of the machine's glass window and includes a mounting plate that allows for coarse positioning of the camera and micrometer stages
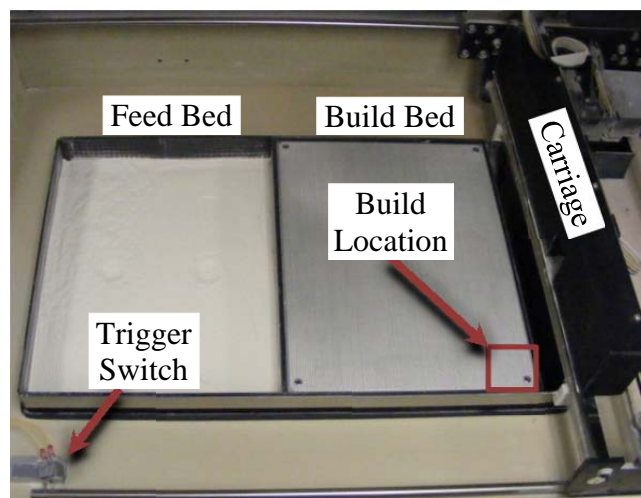
that allow for fine adjustments to the camera location. Photographs of the mounting configuration are shown in Figure 3.
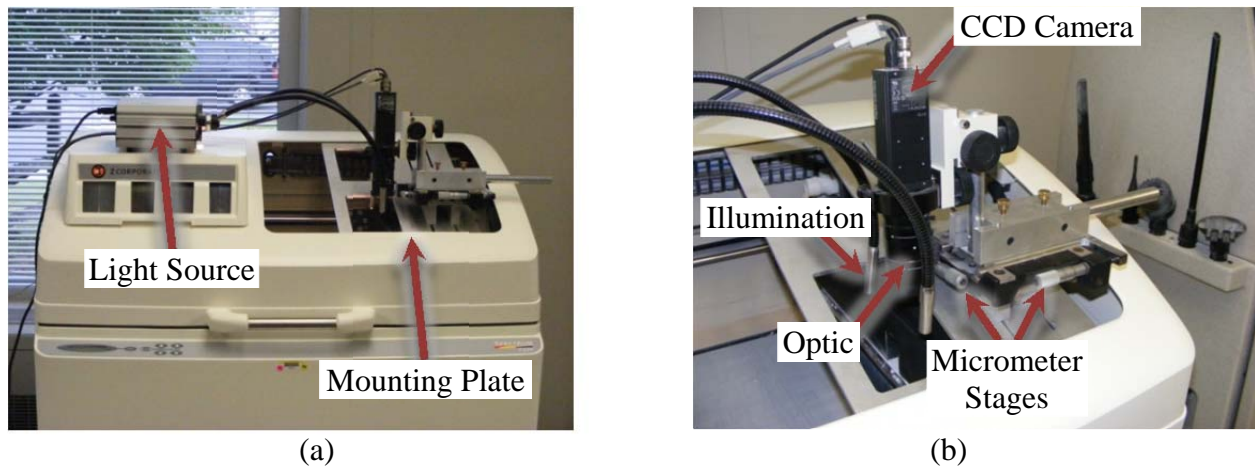
Figure 3: Photographs of the mounting configuration: (a) whole machine and (b) mounting plate.

The camera was triggered by a switch inside the machine that was activated when tripped by the carriage unit. As the powder spreader would reach its full range of travel to the far side of the feed platform, the switch was pressed, and images were acquired after a 100 ms delay to allow time for any vibration to damp out. The camera operation was controlled by a custom LabVIEW program that grabbed the triggered images and saved them to the hard drive.

The build and image acquisition process was as follows: from its starting position to the right of the build bed, the carriage traveled to the left of the feed bed and depressed the camera trigger switch in doing so; after 100 ms, the camera acquired six images that were averaged together, the average image being saved to the computer; the carriage traveled back to the right and introduced another layer of powder onto the build bed; the carriage moved to the left to allow the printheads to travel along the fast axis (front to back) to selectively deposit binder onto the powder bed; and the process repeated. The total number of images to be acquired was predefined so that the very last image was of the very last layer of the build. The build location of the test part was at the right corner closest to the front of the machine. The red box in Figure 4 denotes this location, which was chosen because it allowed imaging of the reference edges of the build

Figure 4: Feed bed, build bed, build location of test part, and trigger switch.

bed, helping to tie the camera's coordinate system to the machine's coordinate system.

Image Processing and Measurement

Settings for the imaging system, illumination, part, and printer were chosen carefully to help minimize any required processing of the captured images. As such, the only steps in processing captured images were to convert the images from 16-bit images to 8-bit images, which was a requirement for the evaluation software, and to average several images. Six images of each layer were captured and averaged together. Any tools used in taking measurements from the images were basic tools available in the image capture and processing software.

The measurements of interest for this study were the positions and geometry of features within each layer of the part. Measurements of feature positions were made relative to reference edges when possible and relative to the first layer when references were unavailable. Both the position and the geometry measurements rely heavily on detecting edges.

There are many algorithms available for edge detection [3]. Edge detection algorithms rely on the intensity profile of a set of pixels, most often a line of pixels. Sub-pixel resolution is available through interpolation of intensities between pixel values and is desirable to help minimize uncertainty. The advanced edge detection method used in this study utilized the zero-crossings of the second derivative of the intensity profile of a specified line of pixels. The intensities are interpolated to one-tenth of a pixel using cubic spline interpolation.

The measurements of interest for our study varied with magnification because of different features seen in the respective fields of view. In magnification A, since the entire part's cross section is in view, the diameters and positions of the inner and outer circles of the cylindrical section were measured. In Figure 6 (a) the upper green circle is the inner circular bound and the lower green circle is the outer circular bound. The edge is expected to be within those bounds. Edges of the circle were detected along the blue spokes spaced at one degree intervals around the entire circle. The yellow dots are the locations of the edges found along the blue spokes, and the red circle is the best-fit circle to all detected edges, which provided the diameters and the center positions. In magnification B, the entire circle is no longer in view, but reference edges appear in the images (see Figure 6 (b)). This allowed measurement of the distance from the edge of the circle to the reference edges. Finally, in magnification C, the position of one edge point was tracked throughout each layer (see Figure 6 (c)). The thick green lines in Figure 6 (b) and (c) are the edge detection line profiles. The smaller green cross lines are where the software detected the edge.

Calibration of the optical measurements entailed estimating the scale factor between pixel distances and real world lengths using a dot grid calibration artifact. The image processing software contained a built-in function to perform this conversion where the user simply had to image the calibration artifact and supply the calibrated distance between the centers of the dots (both in the x and y directions). The software used a non-linear best fit of distances between circle centers measured in pixels and converted that value to a real-world distance based on the user's input. The resolutions were found to be 0.049 mm/pixel, 0.023 mm/pixel, and 0.010 mm/pixel for magnifications A, B, and C, respectively. It should be noted that this method only addresses the average scale factor between image and part coordinates. No correction was made for the possible distortion of the image.
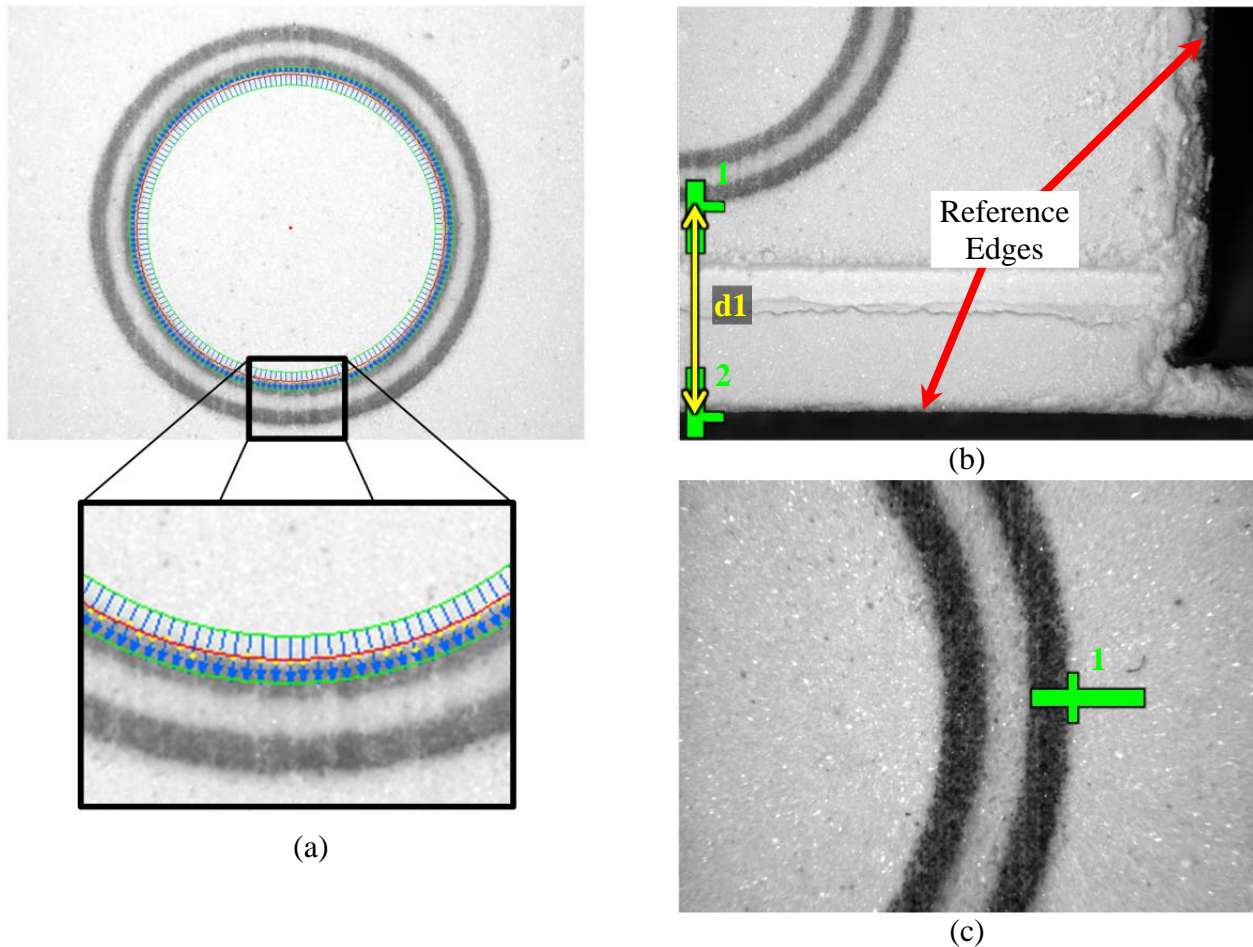
Figure 6:.Screen captures of measurements taken at different magnifications: (a) measurement of the inner circle at magnification A, (b) distance from the part edge to the reference in magnification B, and (c) part edge position in magnification C.

Uncertainty

Uncertainty is a critical component of all measurements. Because the ultimate goal of the current pursuit is process control and improvement, robustness—and therefore uncertainty—are of primary importance. The uncertainty in a measurement is defined in the *Guide to the Expression of Uncertainty in Measurement* [4] as a parameter associated with the result of a measurement that characterizes the dispersion of the values that could reasonably be attributed to the measurand. The parameter may be, for example, a standard deviation (or a given multiple of it), or the half-width of an interval having a stated level of confidence. Uncertainty of measurement comprises, in general, many components. Some of these components may be evaluated from the statistical distribution of the results of a series of measurements and can be characterized by experimental standard deviations. The other components, which also can be characterized by standard deviations, are evaluated from assumed probability distributions based on experience or other information. It is understood that the result of the measurement is the best estimate of the value of the measurand, and that all components of uncertainty, including those

arising from systematic effects, such as components associated with corrections and reference standards, contribute to the dispersion [4].

Determination of the uncertainties in the measurements taken for this study followed a Type A analysis. This means that the method of evaluation of uncertainty is through the statistical analysis of a series of observations [4]. The machine was paused mid-build, and 100 averaged images were acquired of the same exact scene, with each image capture sequence separated by 5 seconds. This was repeated for each magnification setting. The same image processing and measurements performed on individual part layers (as discussed earlier) were performed on each of the 100 averaged images. The standard deviations of the different measurements provide the basis for the uncertainty assessment of each measurement.

It is important to note that camera resolution is a component of measurement uncertainty when making measurements from captured images, but is certainly not the only component of uncertainty. Several components that contribute to the combined measurement uncertainty were evaluated, and efforts were taken to adjust these components to help minimize uncertainty. The results and lessons learned are discussed below. It should be noted that this is not an exhaustive list of phenomena that affect measurement uncertainty.

Edge Detection
The edge detection algorithm allowed adjustment of three settings: contrast, filter size, and steepness. Contrast is the difference between the average pixel intensity on both sides of the edge. An edge only exists if there is a contrast greater than the specified value. Filter width specifies the number of pixels on either side of the edge that are averaged when finding the contrast. Steepness represents the number of pixels that correspond to the transition area of the edge. After testing various settings and combinations, the settings that produced the most reliable edge detection with minimum uncertainty were selected: contrast = 45 graylevels, filter size = 8 pixels, and steepness = 2 graylevels/pixel.

Camera Noise
One of the main sources in uncertainty when utilizing images obtained from a CCD camera is camera noise. Camera noise can be broken down into smaller components (e.g., thermal noise, shot noise, etc.), but for the sake of this project it can be considered, at a higher level, as anything that would cause a slight change in the graylevel intensity of a particular pixel. Since edge detection is executed using pixel intensities, any change or uncertainty in intensity will affect edge detection. To reduce the effects of camera noise, six images were averaged together. When evaluating a characteristic measurement in magnification C, a standard deviation in edge position of 0.77 pixels was determined when using no averaging, and a standard deviation of 0.49 pixels in that same edge position was found when averaging six images together. It would be desirable to average a greater number of images together to further reduce the effect of camera noise. However six images was the maximum number of images that could be collected before the powder spreader returned into the field of view of the camera.

Camera Drift
While the camera fixture and mounting are stable and stiff enough for the purposes of this study, there is still the possibility that the camera could drift, either mechanically or

electronically, relative to the machine coordinate system. To reduce these effects, build position and magnifications were chosen that generally allowed imaging of reference features on the machine (*i.e.*, the edges of the build bed). These reference surfaces not only provide a link between the camera coordinate system and the machine coordinate system, but they also provide a stable base in the machine coordinate system from which to measure distances. Indeed, when measuring in magnification B, one can see the benefits of utilizing reference surfaces. The measurements of the position of the bottom edge of the outer circle have a standard deviation of 1.2 pixels and exhibit a small amount of drift. However, the standard deviation in the vertical distance from that same edge to the bottom reference feature is 0.70 pixels, with less noticeable drift. It should be noted that in magnification C, there are no reference features within view and therefore it is more difficult to determine if any drift in the data is due to movement of the camera relative to the machine reference or movement of the feature relative to the machine reference.
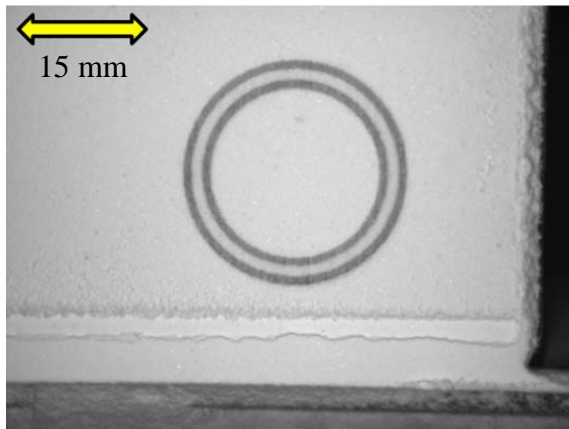
Lighting

It is well known that illumination plays a major role in this type of measurement. To quantify the lighting conditions for analysis, image histograms were employed. The image histograms show the number of pixels that register specific values of grayscale intensity (0 being black and 255 being saturated). Figure 7 shows three different lighting scenarios and their associated histograms. The values of interest were the mean intensity and the number of pixels that had reached saturation.

In general, it was found that brighter lighting (higher intensity) led to lower measurement uncertainties. Comparing the uncertainty in the location of the center of the inner circle in a magnification A scenario, it was found that when the mean intensity was at a grayscale level of 172 (Figure 7 (a)) the standard deviation of the circle center position was 0.038 pixels, while the deviation was 0.031 pixels at a mean graylevel of 190 (Figure 7 (b)), and 0.029 pixels when the mean graylevel was 213 (Figure 7 (c)). The medium level of lighting (mean graylevel of 190) was chosen for future measurements because this setting resulted in only slightly higher uncertainty, but showed very few pixels that reached saturation (pixel saturation can lead to other measurement difficulties like washout). Generally stated, the lighting strategy was to maximize the mean intensity value in the image histogram while keeping a minimal number of saturated pixels.

Part Color

Because the CCD camera only captured grayscale images, part color influenced the uncertainty values. It was desired to build parts that were colored from a single printhead. Yellow, magenta, and cyan parts have a significantly different contrast from the white powder background when imaged in grayscale, as would be expected. This contrast difference affects edge detection. A magenta part produces a smaller contrast than a cyan part. Accordingly, the standard deviation in the center position of the circle in magnification A for a magenta part was 0.101 pixels, while that same feature varied by 0.031 pixels when the part was cyan. This variation in uncertainty would likely not be as great with a color camera that would measure separate intensity values for red, green, and blue. A complication of part color affecting measurement uncertainty is that a multicolored part may have different uncertainty values in
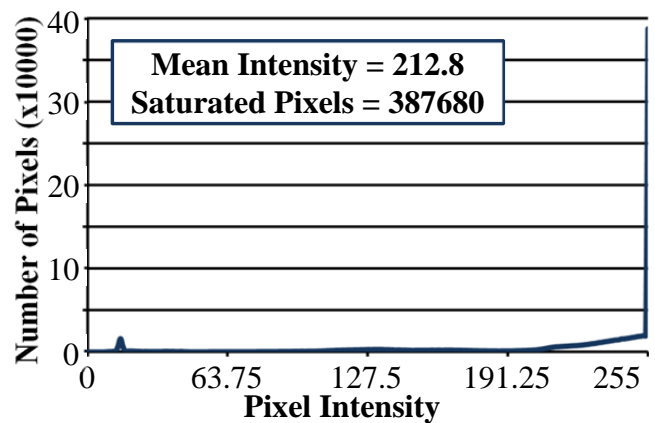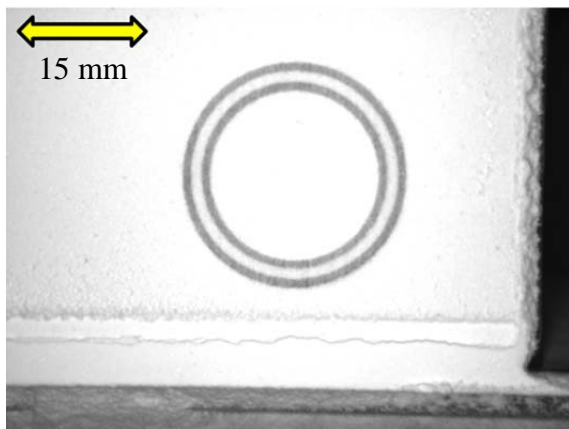
different positions. When transitioning to a metal-based powder bed process, this will likely be less of a problem because of the greater uniformity in appearance of the metal parts.
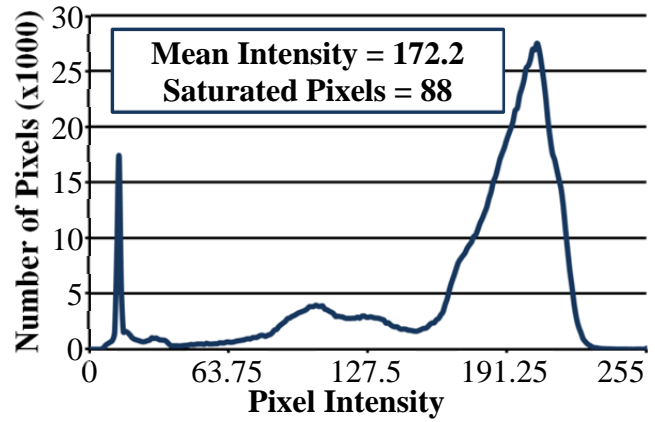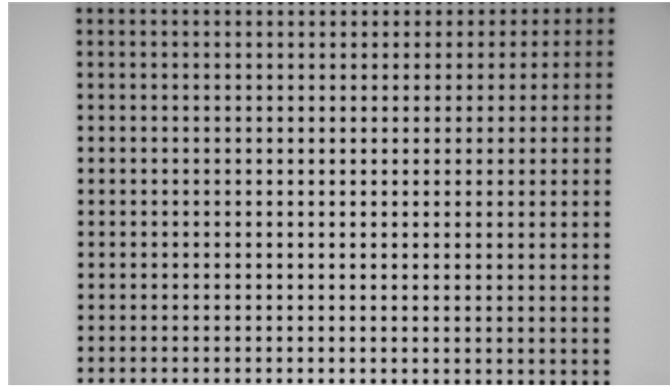

(a)
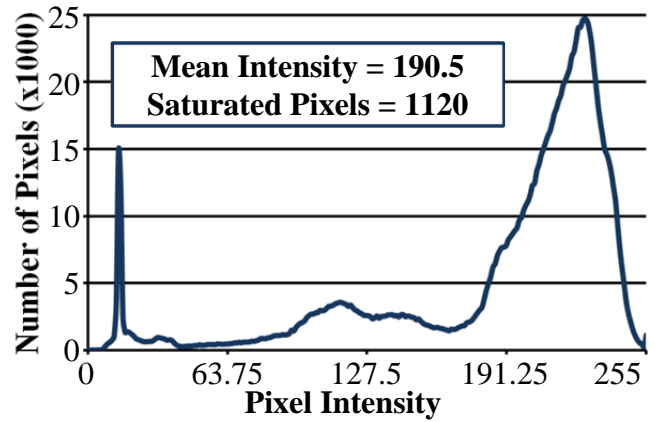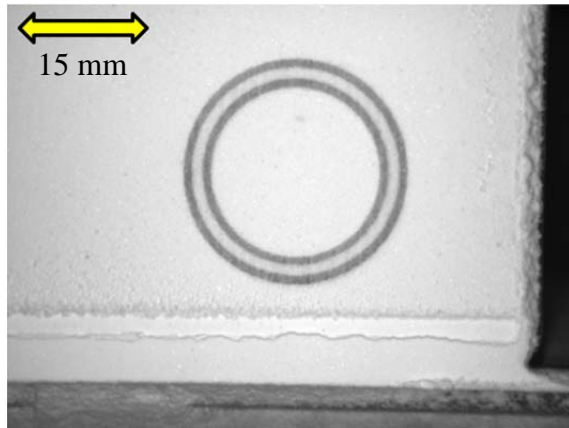
(b)

(c)

Figure 7: Three different lighting scenarios and the associated histograms for scenes with (a) dim lighting, (b) medium lighting, and (c) bright lighting.

Calibration Artifact

The uncertainty due to the calibration artifact differs from the previously mentioned sources of uncertainty in several ways. First, the calibration artifact comes accompanied by a calibration certificate that specifies the size and spacing of the dots in the grid along with the uncertainties in the size and spacing. This is a Type B uncertainty; an uncertainty determined by an evaluation means other than the statistical analysis of series of observations [4]. Second, this source of uncertainty does not, strictly speaking, quantify the robustness of the measurement. Rather, it is a quantification of the uncertainty in conversion from camera coordinates, in pixels, to real world distances, in millimeters. The calibration artifact can be seen in Figure 8.

The expanded uncertainty (k = 2) specified on the calibration data sheet for our dot grid was 0.001 mm in spacing between the dots in both the x and y directions. Expanded uncertainty defines an interval about the measurement result that may be expected to encompass a large fraction of the distribution of values that could reasonably be attributed to the

Figure 8: Calibration artifact at magnification A.

measurand [4]. The variable "k" is the coverage factor, which is multiplied by the standard uncertainty to determine the expanded uncertainty. This uncertainty does not account for mounting the calibration artifact at an improper height or tilt. However, uncertainty due to these sources is assumed to be small enough (cosine of a small angle, which is ≈ 0) to ignore for the purposes of this study.

Combined Uncertainty

The settings that corresponded to the minimum measurement uncertainty were selected for each input discussed, and 100 averaged images in each magnification were acquired and analyzed. The expanded uncertainties (k = 2) for the measurements of interest are shown in Table 2.

Table 2: Expanded uncertainties.

Measurement	Magnification	Expanded Uncertainty (mm)
Diameter	A	0.047
Edge distance from reference	B	0.032
Edge position	C	0.010

The uncertainty for magnification A is likely sufficient for geometrical measurements of parts made on the current 3D printer. However, the uncertainty values for magnifications B and C are more problematic because these measurement scenarios are intended more for process control and improvement, and uncertainty for control should be an order of magnitude smaller

than uncertainty for geometry. Furthermore, when considering that metal parts and machines producing metal parts will likely require much smaller tolerances, still smaller measurement uncertainty is desired.

Measurements

Measurements were made at three different magnifications. Magnification A had a resolution of 0.049 mm/pixel, magnification B had a resolution of 0.023 mm/pixel, and magnification C had a resolution of 0.010 mm/pixel. Measurements made at magnification A are most likely to be used to evaluate the geometry of a part during the build process. Measurements at magnification B and magnification C would likely be more pertinent to process control than geometry because of the smaller uncertainties and the fact that a small percentage of the part's geometry is in view at these higher magnifications.

Geometry
The diameters of the inner and outer circles of the cylindrical feature were measured (see Figure 6 (a)). Half the difference between the diameters was taken as the wall thickness. Figure 9 depicts the measurements of the outer and inner diameters, as well as the wall thickness of the printed part.

The average outer diameter was 24.669 mm, the average inner diameter was 18.846 mm, and the average wall thickness was 2.912 mm, 0.088 mm smaller than the part's design. After the part was finished, it was baked at 88 °C for two hours. The baked part was measured on a CMM using an 8 mm diameter probe at the end of a 50 mm shank. Outer and inner diameters were measured on the CMM at 5 heights: 15.0 mm, 17.5 mm, 20.0 mm, 22.5 mm, and 25.0 mm (corresponding to layer numbers 147, 172, 196, 221, and 245). The average outer diameter measured by the CMM was 24.887 mm, the average inner diameter was 18.810 mm, and the average wall thickness was 3.038 mm, 0.038 mm larger than the part's design. The expanded uncertainty of a length measurement on the CMM is 0.0034 mm over 450 mm of travel.

The measurements using the process intermittent images generally agree with the CMM measurements, but are not equal. This was expected. The process intermittent measurements are of individual layers. Since the ball of the CMM's stylus was not as small in diameter as the thickness of the 100 micrometer layers, the measurement at a layer's height will be larger than the actual layer width if the neighboring layers protrude further out of the part. By how much is determined by the stylus tip size. Therefore, the CMM contacts the most extended layer. Figure 10 is a schematic of this phenomenon. As such, for a part whose layer position varies, the wall thickness measurement is expected to be larger on the CMM than on the process intermittent images. It is important to note, however, that CMM measurements of additively manufactured parts are still useful. If the part were a boss, for example, then the overall maximum measurements can be used to determine whether or not a mating part would fit.
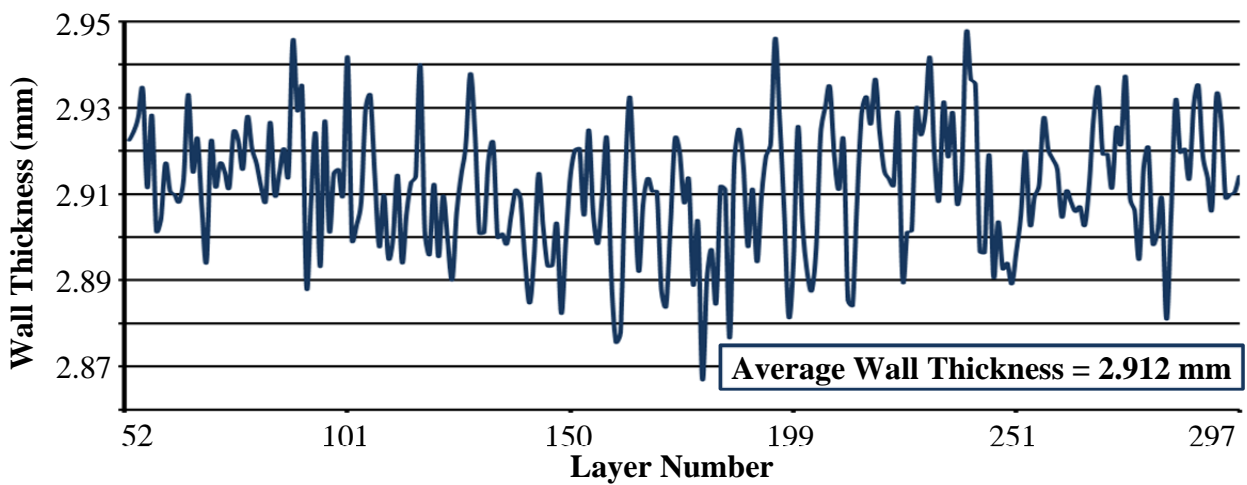
The baked parts were dipped in cyanoacrylate to infiltrate and strengthen them. The infiltrated part was returned to the CMM and determined to have an average outer diameter of 24.896 mm, an average inner diameter of 18.719 mm, and an average wall thickness of 3.088 mm, 0.088 mm larger than the part's design. This means that, accounting for post-processing and
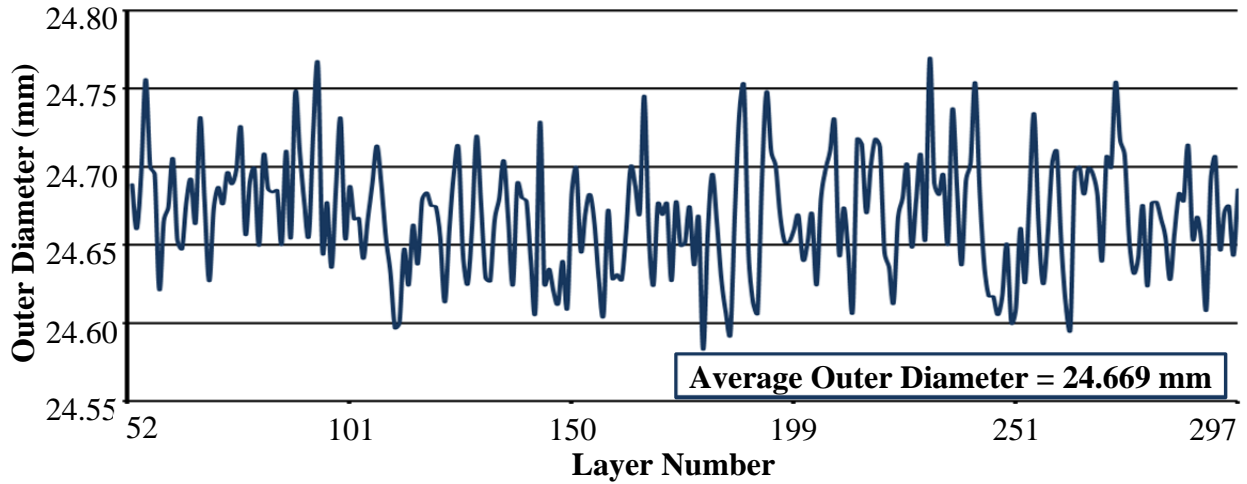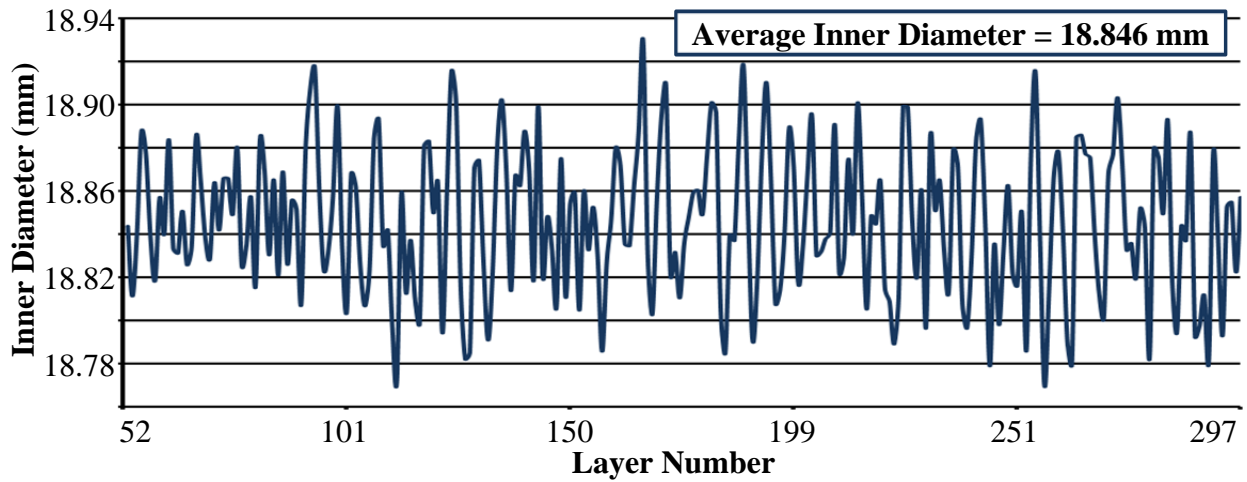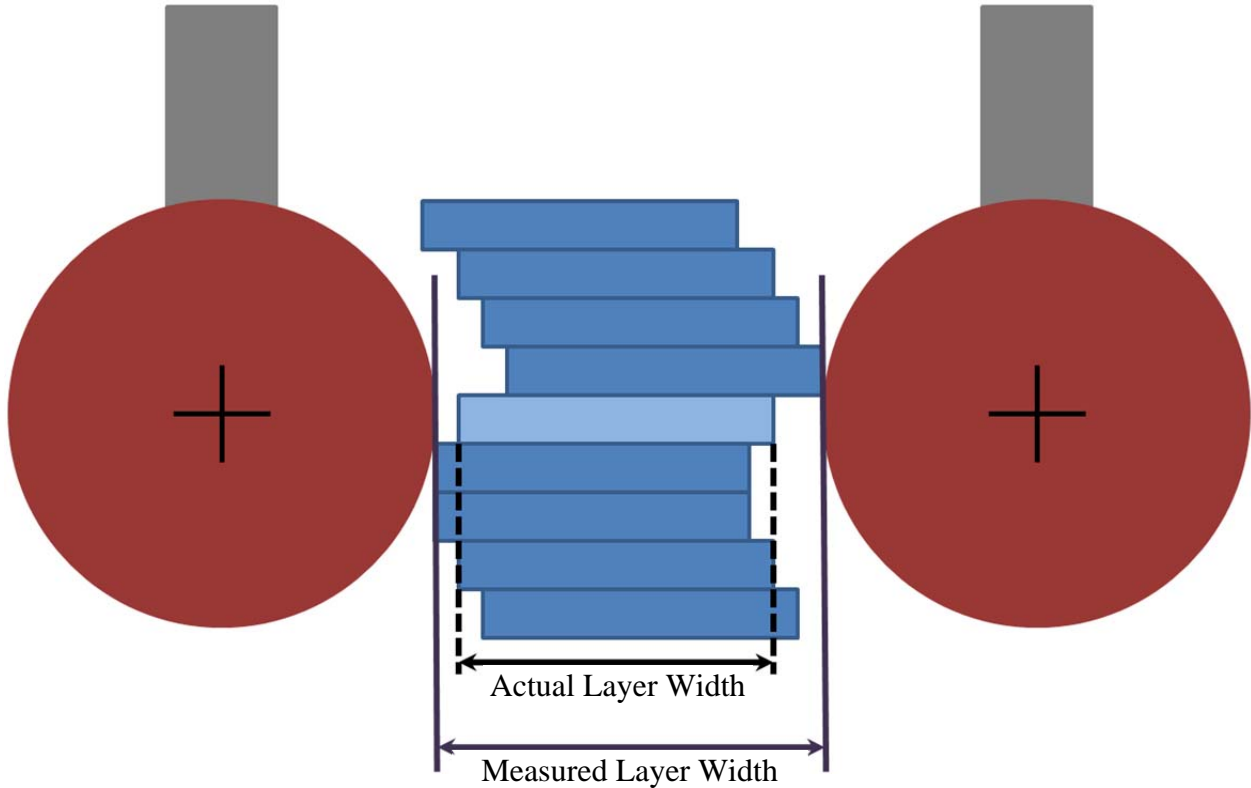
Figure 9: Charts depicting the (a) outer diameter, (b) inner diameter, and (c) wall thickness as measured in process intermittent images.

**Figure 10:** Schematic of the measurement error due to the probe radius.

the CMM measurement phenomenon, the geometry of the examined part measured in process intermittent images maps to the final part dimensions at a ratio of 2.912:3.088, or 94 percent. Therefore, in this case, if the final part's wall thickness measurement is meant to be 3 mm, the process intermittent image measurements must average to be approximately 2.83 mm.

Process

A process that is well-controlled is predictable and repeatable. As such, we measured feature position and geometry at each layer to examine the consistency with which the circular layers in the cylindrical portion of the part were produced.

Results illustrating consistency of part outer and inner diameters were shown earlier in Figure 9 (a) and (b). Figure 11 (a) and (b) show results of the position of the outer edge of the part, and further confirm that the layers vary by a significant amount, approximately 0.150 mm (standard deviation). Furthermore, the layer positions appear to oscillate..

External edge positions should contribute directly to the surface roughness of the part. To examine this, a stylus profilometer was used to measure the surface profile of test parts. The intention was to illustrate the deviations in layer position. Figure 12 shows the surface profile of a part measured at magnification C.

(a)

(b)
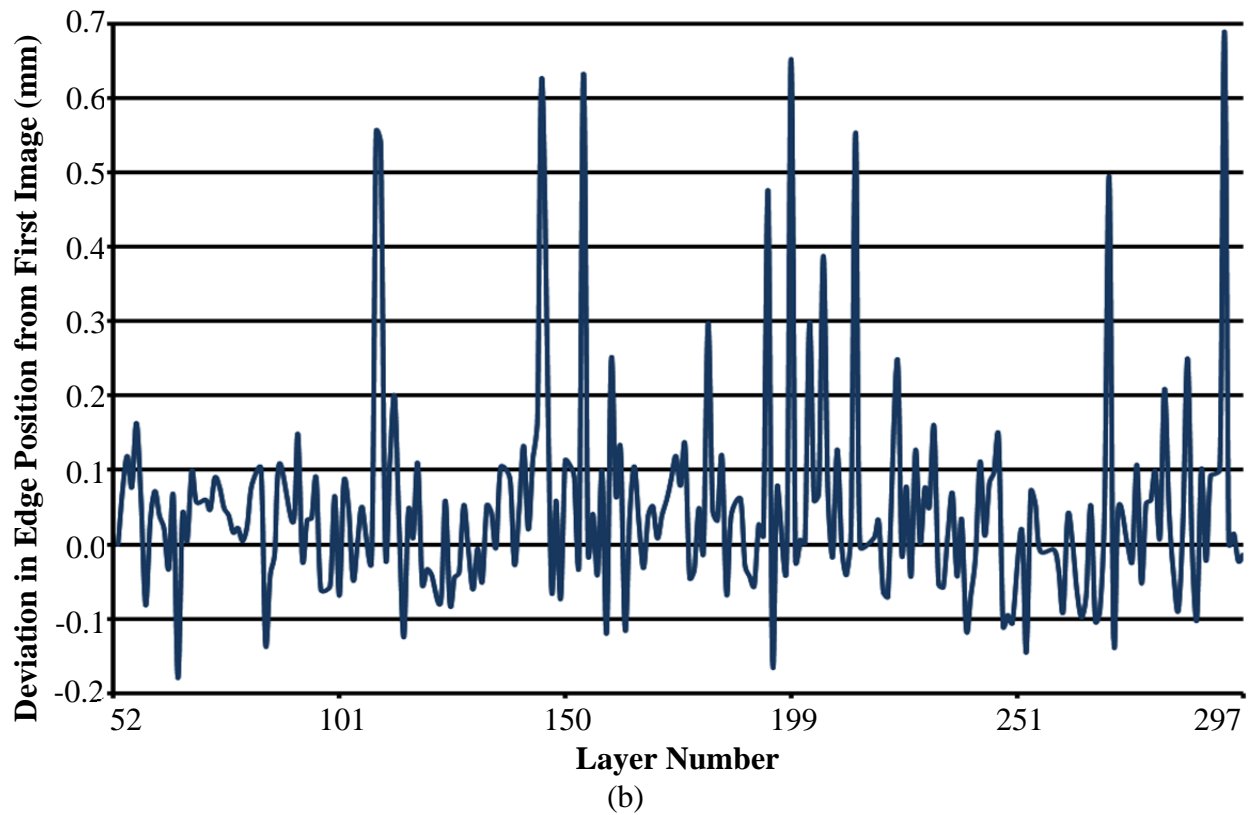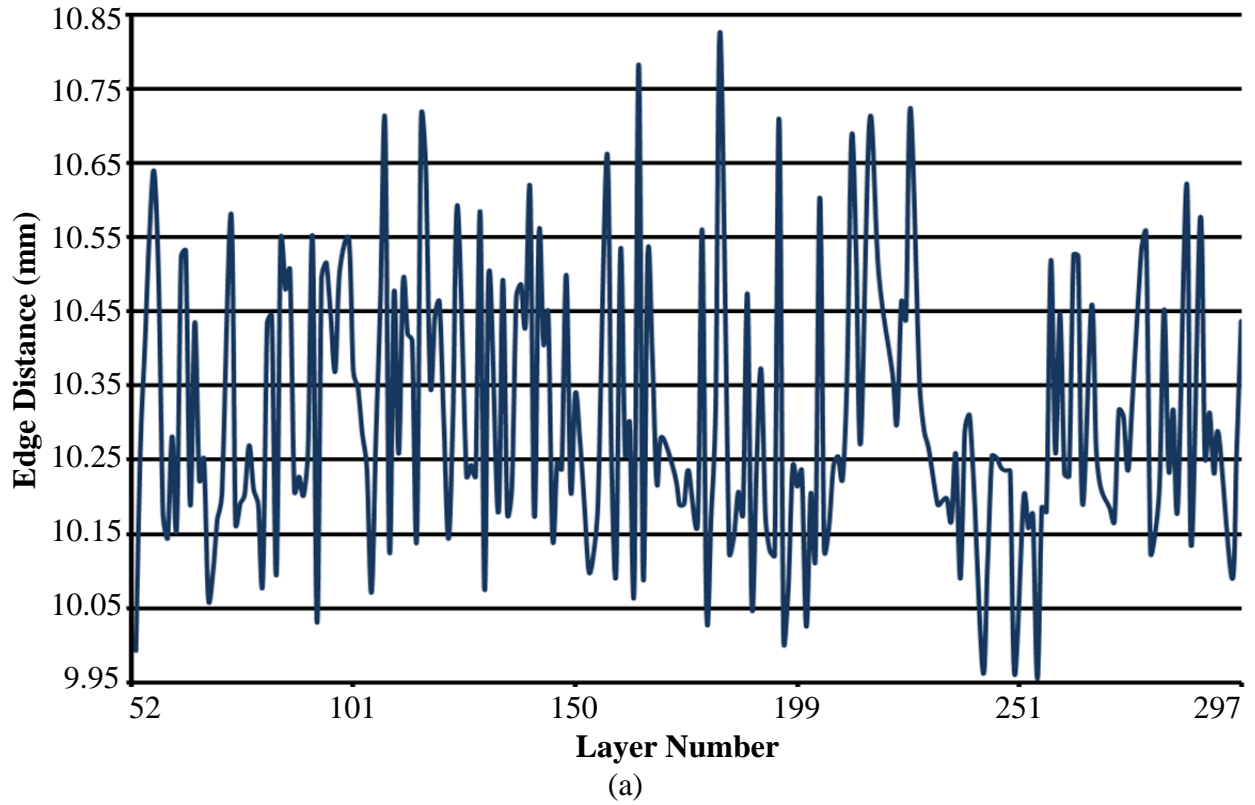
Figure 11: Charts depicting (a) distance of test part to reference edge in magnification B images and (b) deviations from the first image taken at magnification C.
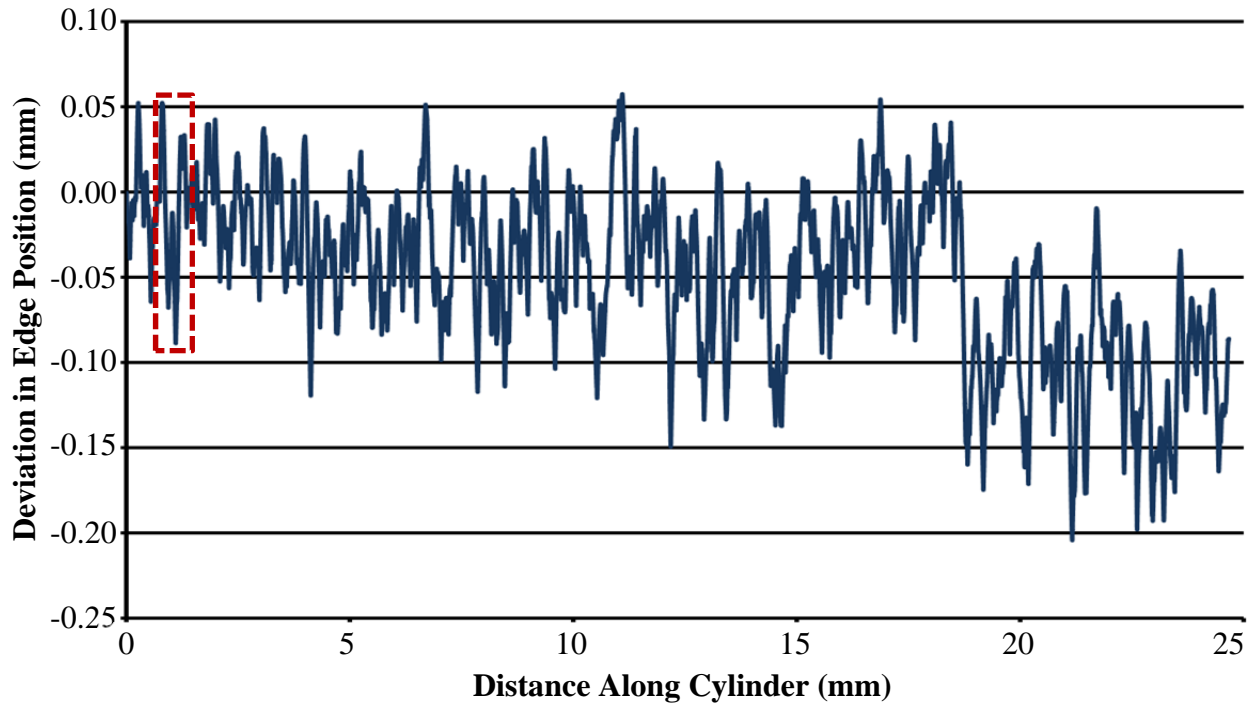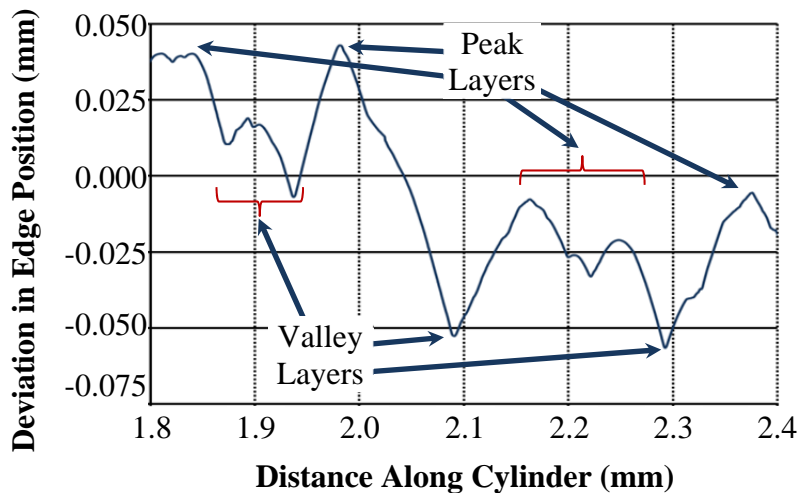
Figure 12: Profilometer measurement of test part captured at magnification C: (a) full scan and (b) zoomed in section showing alternating layer position.

Matching the location of the profilometer measurement with the location of the edge position measurement proved difficult. Because of this, the profilometer measurements do not match the image measurements. Additionally, the smaller magnitude of the profilometer measurements may be due to interference from the stylus shank and the stylus not being normal to the surface. However, profilometer measurements confirm the presence of layer oscillations.

The microscope images in Figure 13 exhibit further evidence of the oscillating nature of the layer positions. Part images i and ii of Figure 13 (a) are captured at a 5x magnification, and the corresponding part images of Figure 13 (b) are captured at a magnification of 10x. The i images of the figure have the peaks of the test part's surface in focus, while the ii images have the valleys of the test part's surface in focus. The red, dashed lines are provided to aid in discerning the in-focus and out-of-focus portions of the images. This figure is demonstrative of the oscillatory effect. It is important to note, however, that each band in focus is larger than the 0.100 mm layer thickness. Although there was a slight deviation from the programmed 0.100 mm layer thickness, the deviation was not large enough to support a claim that each band in the image represents one layer.

These microscope images also make visible the granularity of the test part's surface. It is this granular structure that makes further analysis with confocal microscopy and scanning white light interferometry exceedingly difficult, since the rough surface scatters any incoming light,
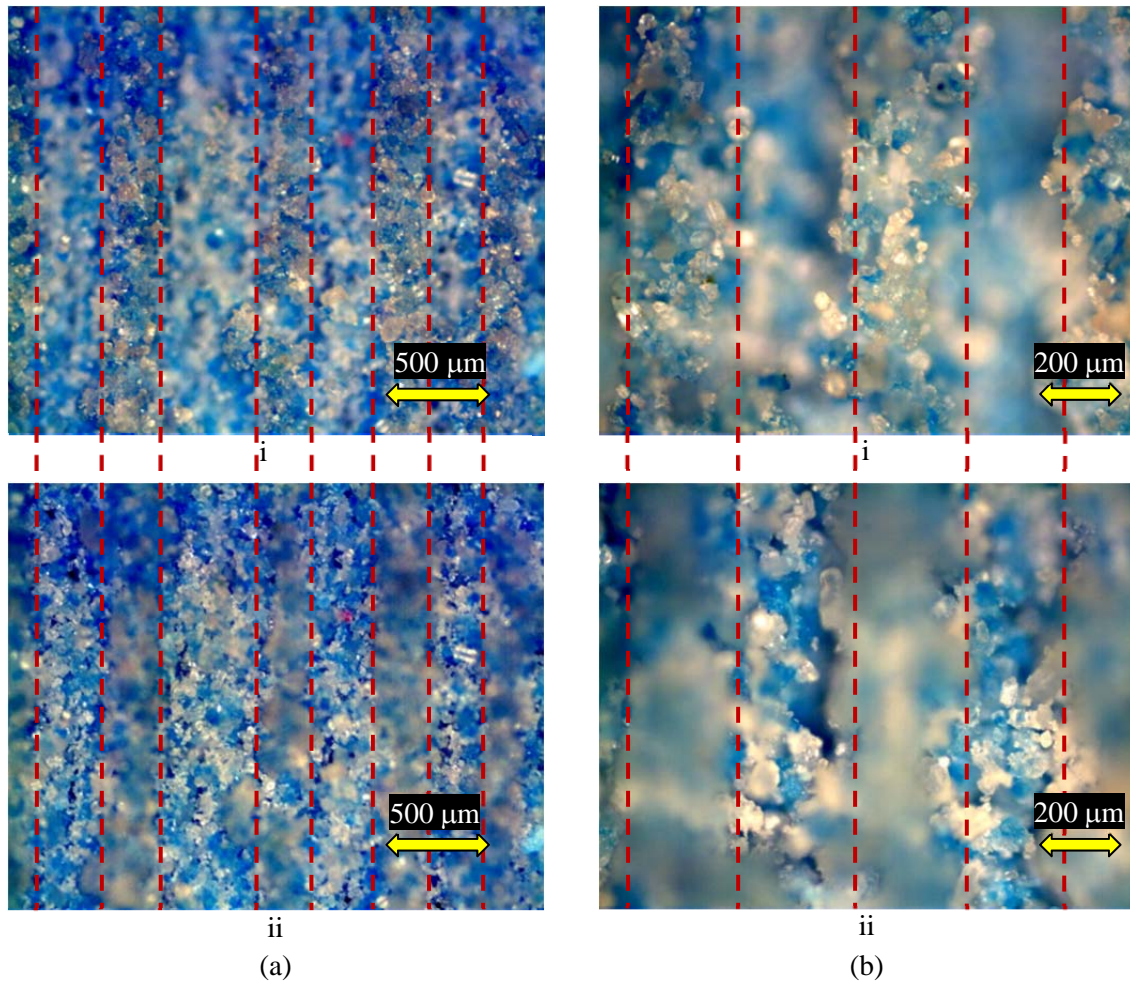
Figure 13: Microscope images that demonstrate the alternating nature of the layer positions at a magnification of (a) 5x and (b) 10x; the i images have peaks of the test part's surface in focus, while the ii images have the valleys of the test part's surface in focus.

and the little light returning to the sensor for measurement is inadequate. Also, it is probable that the individual grains account for the higher frequency component of the profilometer measurements.

Conclusions

Process intermittent measurements with characterized uncertainties are presented here. Uncertainty analysis is important in characterizing the robustness of a measurement process. This study employed three different magnifications, which resulted in pixel resolutions of 0.049 mm/pixel, 0.023 mm/pixel, and 0.010 mm/pixel. The expanded uncertainty for the first magnification is 0.047 mm. Results at this magnification are useful for predicting the final part geometry. Comparing process intermittent measurements of geometry with post-process measurements of the same geometry shows an expected undersizing of the process intermittent measurement. The expanded uncertainty for magnification B is 0.032 mm. This magnification, along with magnification C, for which the expanded uncertainty is 0.010 mm, are more likely to be used for performing process control. If the process could be controlled to 0.010 mm, then accuracy of parts made by additive manufacturing would likely improve from the 0.050 mm – 0.100 mm errors seen in previous research [5]. However, measurement uncertainty of 0.010 mm does not imply that the process can be controlled to that same level. As such, work in improving measurement uncertainty and process control is ongoing. Additionally, the methods outlined in this work will be applied to measurements on a metal-based additive process in the future.

Acknowledgements

References

[1] Bourell, D.L., Leu, M.C., and Rosen, D.W., 2009, *Roadmap for Additive Manufacturing: Identifying the Future of Freeform Processing*.

[2] Gatto, M. and Harris, R.A., 2011, Non-destructive analysis (NDA) of external and internal structures in 3DP, *Rapid Prototyping Journal*, 17(2), 128-137.

[3] Ziou, D. and Tabbone, S., 1998, Edge Detection Techniques - An Overview, *International Journal of Pattern Recognition and Image Analysis*, 8(4), 537-559.

[4] Joint Committee for Guides in Metrology, 2008, *Evaluation of measurement data — Guide to the expression of uncertainty in measurement (GUM)*.

[5] Cooke, A.L., Soons, J.A., 2010, Variability in the Geometric Accuracy of Additively Manufactured Test Parts, *21st International Solid Freeform Fabrication Symposium – An Additive Manufacturing Conference*, August 2010, Austin, TX, 1-12.